






7T dynamic contrast-enhanced MRI for the detection of subtle blood–brain barrier leakage

Lisanne P. W. Canjels^{1,2,3}  | Jacobus F. A. Jansen^{1,2,3}  | Marieke van den Kerkhof^{1,2}  |
 Robert-Jan Alers^{4,5} | Benedikt A. Poser⁶ | Christopher J. Wiggins⁷ |
 Veronique M. M. M. Schiffer^{4,5} | Vincent van de Ven⁶ | Rob P. W. Rouhl^{2,8,9} |
 W. M. Palm¹ | Robert J. van Oostenbrugge^{2,8,10} | Albert P. Aldenkamp^{2,3,8,9} |
 Chahinda Ghossein-Doha^{5,10,11} | Marc E. A. Spaanderman^{4,5} | Walter H. Backes^{1,2,10}

¹ Department of Radiology and Nuclear Medicine, Maastricht University Medical Center, Maastricht, the Netherlands

² MHENS, School for Mental Health and Neuroscience, Maastricht University, Maastricht, the Netherlands

³ Department of Electrical Engineering, Eindhoven University of Technology, Eindhoven, the Netherlands

⁴ Department of Gynecology and Obstetrics, Maastricht University Medical Center, Maastricht, the Netherlands

⁵ GROW, School for Oncology and Developmental Biology, Maastricht University, Maastricht, the Netherlands

⁶ Faculty of Psychology and Neuroscience, Maastricht University, Maastricht, the Netherlands

⁷ Scannexus BV, Maastricht, the Netherlands

⁸ Department of Neurology, Maastricht University Medical Center, Maastricht, the Netherlands

⁹ Academic Center for Epileptology Kempenhaeghe/Maastricht UMC+, Heeze and Maastricht, the Netherlands

¹⁰ CARIM, School for Cardiovascular Diseases, Maastricht University, Maastricht, the Netherlands

¹¹ Department of Cardiology, Maastricht University Medical Center, Maastricht, the Netherlands

Correspondence

Walter H. Backes, Ph.D., Department of Radiology and Nuclear Medicine, Maastricht University Medical Center, PO Box 5800, 6202 AZ Maastricht, the Netherlands.
 Email: w.backes@mumc.nl

Abstract

Background and Purpose: Dynamic contrast-enhanced MRI (DCE-MRI) can be employed to assess the blood–brain barrier (BBB) integrity. Detection of BBB leakage at lower field strengths (≤ 3 T) is cumbersome as the signal is noisy, while leakage can be subtle. Utilizing the increased signal-to-noise ratio at higher field strengths, we explored the application of 7T DCE-MRI for assessing BBB leakage.

Methods: A dual-time resolution DCE-MRI method was implemented at 7T and a slow injection rate (0.3 ml/s) and low dose (3 mmol) served to obtain signal changes linearly related to the gadolinium concentration, that is, minimized for T_2^* degradation effects. With the Patlak graphical approach, the leakage rate (K_i) and blood plasma volume fraction (v_p) were calculated. The method was evaluated in 10 controls, an ischemic stroke patient, and a patient with a transient ischemic attack.

Results: K_i and v_p were significantly higher in gray matter compared to white matter of all participants. These K_i values were higher in both patients compared to the control

This is an open access article under the terms of the [Creative Commons Attribution-NonCommercial](https://creativecommons.org/licenses/by-nc/4.0/) License, which permits use, distribution and reproduction in any medium, provided the original work is properly cited and is not used for commercial purposes.

© 2021 The Authors. *Journal of Neuroimaging* published by Wiley Periodicals LLC on behalf of American Society of Neuroimaging



subjects. Finally, for the lesion identified in the ischemic stroke patient, higher leakage values were observed compared to normal-appearing tissue.

Conclusion: We demonstrate how a dual-time resolution DCE-MRI protocol at 7T, with administration of half the clinically used contrast agent dose, can be used for assessing subtle BBB leakage. Although the feasibility of DCE-MRI for assessing the BBB integrity at 3T is well known, we showed that a continuous sampling DCE-MRI method tailored for 7T is also capable of assessing leakage with a high sensitivity over a range of K_i values.

KEYWORDS

blood–brain barrier, cerebrovascular disease, DCE-MRI, 7T

INTRODUCTION

Dynamic contrast-enhanced MRI (DCE-MRI) is a commonly used technique to determine the functional integrity of the blood–brain barrier (BBB).¹ Since the first application, it has proven valuable in different brain pathologies with disruption of the BBB, such as high-grade tumors,² multiple sclerosis (MS),³ and acute ischemic stroke.⁴ While these pathologies show a relatively large BBB leakage in lesions, more recently the application of DCE-MRI in pathologies with more subtle BBB leakage, such as cerebral small vessel disease⁵ and Alzheimer's disease,⁶ has been demonstrated.

Leakage of contrast agents (CAs) into the brain can be very subtle and the level of signal enhancement due to leakage is gradual, small, and noisy. The use of ultra-high field strengths ($> 3T$) compared to the clinical standard (3T) can have several advantages for DCE-MRI. First, the native tissue relaxation rate, R_1 , decreases with field strength, and its relative value changes, therefore, more easily to CA uptake. Additionally, the larger magnetization provides a higher signal-to-noise ratio (SNR), which can be used to obtain a higher spatial resolution and/or higher temporal resolution.⁷ The relationship between SNR, spatial and temporal resolution is a trade-off and therefore it is not always possible to optimize all characteristics as longer acquisition (repetition) times might be required to keep the specific absorption rate within limits.^{7,8} Furthermore, increased (B_0 and B_1) field inhomogeneities, lower relaxivity of the CA, and magnetic susceptibility artifacts of the bolus may counteract these beneficial properties of 7T MRI.^{7,9} Therefore, it needs to be investigated whether DCE-MRI at 7T enables sufficient sensitive detection of subtle leakage.

During a DCE-MRI examination, a paramagnetic CA is intravenously administered and the resulting changes in signal intensity are followed over time. To increase the sensitivity for the detection of low CA concentrations, T_1 -weighted images are continuously acquired before, during, and over a longer period of time (>15 min) after CA administration.^{3,10} A compromised BBB allows the CA to leak into the brain tissue, leading to an increased signal intensity on T_1 -weighted images. By relating the temporal changes in CA concentration in the brain parenchyma to the blood concentrations using pharmacokinetic modeling, measures of the BBB leakage are calculated.^{11,12} Although at lower magnetic fields, DCE-MRI has been proven to be capable of visu-

alizing and quantifying BBB leakage, to our knowledge, the potential of a continuous sampling DCE-MRI method at 7T combined with pharmacokinetic modeling to quantify subtle BBB leakage has not been investigated.

The aim of this study was to develop a continuous sampling, dual-time resolution 7T DCE-MRI protocol for measuring subtle BBB leakage. Here, we describe the developed DCE-MRI protocol with image acquisition parameters, contrast injection settings, theoretical signal calculations, and pharmacokinetic modeling. The protocol was evaluated in 10 healthy control subjects and two patients with cerebrovascular disease to capture a large leakage range.

METHODS

MRI

Images were acquired with a 7T MRI System (Magnetom, Siemens Healthineers, Erlangen, Germany) equipped with a 32-channel phased-array head coil (Nova Medical coil, Wilmington, MA, USA). Dielectric pads were placed in the proximity of the temporal lobe to improve B_1 field homogeneity across the brain.¹³ Moreover, to track potential signal drift, 1.5 ml Eppendorf tubes filled with 0.3 mM Gadobutrol, that is, gadolinium phantom vials, were placed posteriorly to the neck. The DCE-MRI protocol consisted of B_1^+ mapping, a T_1 -weighted sequence to image the anatomy, and the DCE-scan, see Figure 1.

A fluid attenuated inversion recovery (FLAIR) sequence (repetition time [TR]/echo time [TE]/inversion time [TI]: 8000/303/2330 ms; field of view [FOV]: $192 \times 192 \times 176$ mm³; voxel size: $1 \times 1 \times 1$ mm³, acquisition time: 6:59 min:s) was applied to facilitate optimal segmentation of white and gray matter. To accurately identify stroke lesions, a T_2 -weighted sequence (TR/TE: 4000/283 ms; FOV: $192 \times 192 \times 176$ mm³; voxel size: $0.75 \times 0.75 \times 0.75$ mm³, acquisition time: 6:22 min:s) was acquired.

Before the T_1 -weighted DCE-MRI sequence was applied, a Saturation-prepared with 2 Rapid Gradient Echoes (Sa2RAGE) sequence (TR/TE: 2400/0.78 ms, T_{11}/T_{12} : 58/1800 ms, flip angle $[\alpha]_1/\alpha_2$: $4^\circ/10^\circ$, voxel size: $2 \times 2 \times 2$ mm³ and generalized autocalibrating partially parallel acquisitions [GRAPPA] factor: 2) was performed

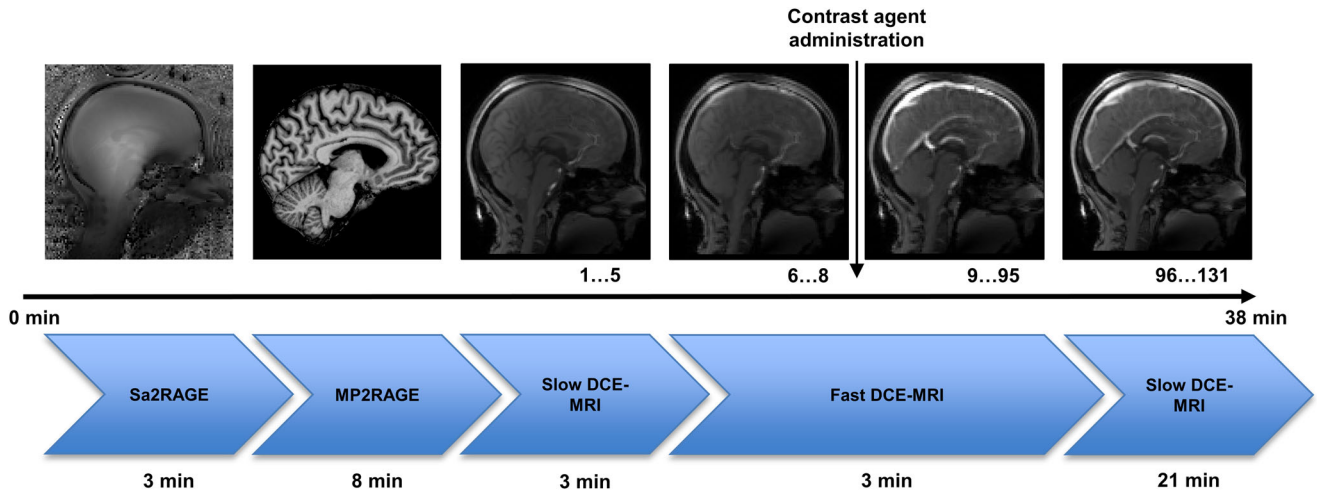


FIGURE 1 Timeline of the imaging protocol with example images and acquisition time. The administration of the contrast agent is denoted with the vertical arrow. The number of dynamic phases is stated under the MR images. Abbreviations: DCE-MRI, dynamic contrast-enhanced MRI; Echoes; MP2RAGE, Magnetization-Prepared 2 Rapid Acquisition Gradient Echo; min, minutes; Sa2RAGE, Saturation-prepared with 2 Rapid Gradient

for B_1^+ mapping across the brain to correct for the low signal, particularly in the temporal lobe. Also, T_1 mapping of the native brain tissue was performed to enable conversion of the contrast-enhanced signal intensity time-series to CA concentrations. For this, a 3D T_1 -weighted Magnetization-Prepared 2 Rapid Acquisition Gradient Echo (MP2RAGE) sequence was applied to obtain whole-brain quantitative T_1 images (TR/TE: 5000/2750 ms, T_{11}/T_{12} : 900/2750 ms; α_1/α_2 : $5^\circ/3^\circ$; voxel size: $0.7 \times 0.7 \times 0.7$ mm³; GRAPPA: 3 and acquisition time: 8 min).¹⁴

For BBB leakage detection, the DCE-MRI protocol utilized two nested pulse sequences to provide a dual-time resolution^{3,6}: a fast (during contrast) continuous dynamic scan (dynamic scan interval of 1.86 s) to measure the rapid signal changes of the early blood circulations of the CA, and a slow dynamic scan (dynamic scan interval of 34 s, measured pre and postcontrast) to sample the baseline signal and the slow extravasation of the CA into the tissue. Both pulse sequences comprised a T_1 -weighted spoiled 3D gradient echo (volumetric interpolated brain examination) sequence. While the pre and postcontrast part was acquired with full brain coverage, the during contrast sequence was acquired for a smaller slab area of the brain that was sagittally positioned through the superior sagittal sinus (SSS) (Figure 2). This narrower coverage was required to achieve a shorter dynamic scan interval. The acquisition parameters of this sequence are specified in Table 1.

After the first three volumes were acquired with the fast (during contrast) DCE-MRI sequence, the CA (1.0 M gadobutrol, 3 ml) was injected into the antecubital vein with a power injector, at a low flow rate of 0.3 ml/s, followed by a 20 ml saline flush. Due to this slow injection rate, the bolus peak appeared approximately at the 30th dynamic of the fast (during contrast) part of the DCE-MRI sequence and T_2^* signal degrading effects were minimized.

DCE-MRI protocol setup

The efficacy of CAs is not just controlled by their pharmacokinetic properties, such as distribution and concentration, but also by the intrinsic magnetic properties of the CA, that is, relaxivity.⁹ The relationship between signal intensity (SI) enhancement and CA concentration in blood, white (WM), and gray matter (GM) was calculated using the signal equation for a fast-spoiled gradient echo sequence:

$$SI = k \frac{\sin \alpha (1 - e^{-TR/T_1})}{(1 - \cos \alpha \cdot e^{-TR/T_1})} e^{-TE/T_2^*} \quad (1)$$

where k is a scaling factor depending on proton density and machine factors, α is the flip angle, TR is the repetition time, and TE is the echo time. Finally, T_1 and T_2^* are the longitudinal and transverse relaxation times, respectively, with:

$$\frac{1}{T_i} = \frac{1}{T_{i,0}} + [CA] \cdot r_i \quad (2)$$

In this equation, $T_{i,0}$ is either $T_{1,0}$ or $T_{2,0}^*$, the native (precontrast) tissue relaxation times, $[CA]$ is the contrast agent concentration, and r_i is the relaxivity constant of the CA. For the computer calculations, the parameters were set at: $\alpha = 6.5^\circ$, TR = 3.7 ms, TE = 1.3 ms, $T_{1,0,\text{blood}} = 2300$ ms,¹⁵ $T_{2,0}^*,\text{blood}} = 33$ ms,¹⁵ $T_{1,\text{WM}} = 1300$ ms,^{16,17} $T_{1,\text{GM}} = 2000$ ms,^{16,17} $r_1 = 4.2$ mM⁻¹s⁻¹,¹⁵ and $r_2 = 6.5$ mM⁻¹s⁻¹.⁹

The relationship between signal intensity and concentration is non-linear in general. Only for very low concentrations, which holds for the brain parenchyma,^{18,19} the relation can be approximated by the linear relation:

$$\frac{SI - S_0}{S_0} = r_1 \cdot T_{10} \cdot [CA] \quad (3)$$

FIGURE 2 Representative example of acquired skull-stripped T_1 -maps (A1, A2, and A3), images of the fast (during contrast) DCE-MRI part at the highest contrast agent concentration (B1, B2, and B3), and first dynamic phase of the slow (postcontrast) DCE-MRI part after contrast agent arrival (C1, C2, and C3). While full brain coverage was obtained for the slow (pre and postcontrast) DCE-MRI parts, a smaller brain area (yellow border lines), planned with the middle slice through the superior sagittal sinus, was acquired for the fast (during contrast) part to obtain shorter dynamic scan intervals.

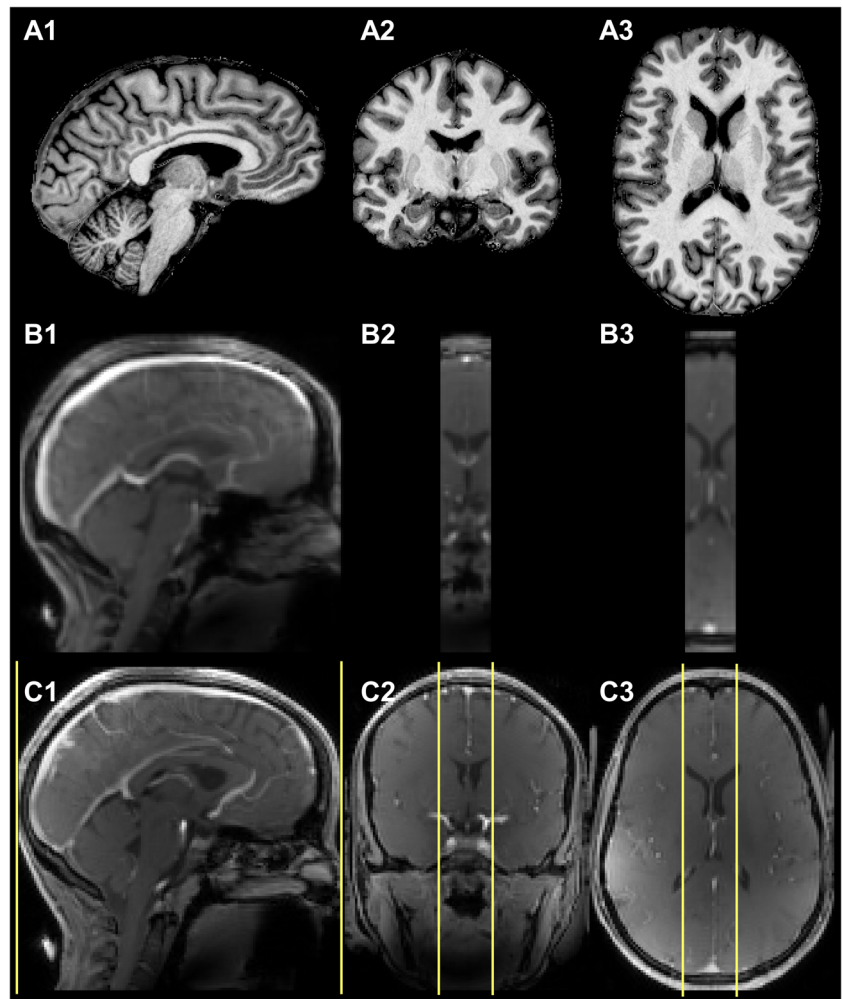


TABLE 1 DCE-MRI scan parameters

	Precontrast	Fast (during contrast) scan	Postcontrast
TR/TE (ms)	3.7/1.3	3.7/1.3	3.7/1.3
α ($^{\circ}$)	6.5	6.5	6.5
Voxel size (mm)	1.5 \times 1.5 \times 1.5	2.0 \times 2.0 \times 2.0	1.5 \times 1.5 \times 1.5
Field of view (mm)	192 \times 192 \times 144	192 \times 192 \times 32	192 \times 192 \times 144
Dynamic scan interval (s)	34	1.86	34
Number of dynamics	5	90	36
Acquisition time (min:s)	2:50	2:47	20:24

Abbreviations: α , flip angle; min, minute; mm, millimeter; ms, millisecond; TE, echo time; TR, repetition time.

where S_0 is the native tissue signal intensity. The T_2^* effect was neglected in WM and GM. When CA concentrations become higher, as for instance, in the blood stream, the signal intensity is in the non-linear range and might be influenced by T_2^* -related signal decay. In this situation, CA concentrations cannot be estimated accurately. For instance, in blood, a 1% difference between the signal enhancement

with and without the T_2^* -related signal decay (black lines in Figure 3A) is obtained at a concentration of 0.45 mM. For GM, 1% difference between the theoretical signal enhancement and the linear relation is calculated at a 10 times lower concentration of 0.048 mM, while in WM, this is at 0.032 mM. These computational estimations serve to provide highest concentration levels for which the linear relation holds.

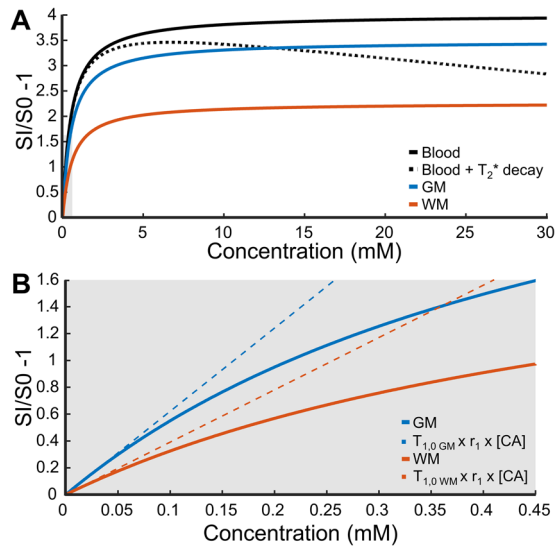


FIGURE 3 (A) Illustration of the calculated relation between signal enhancement and contrast agent (CA) concentration in blood (black), gray matter (GM, blue), and white matter (WM, orange). The T_2^* effect was negligible in WM and GM, but not in blood (black dotted line). In the first part of the black dotted line, the T_2^* effect is neglectable. (B) Magnification of the theoretical relation between signal enhancement and contrast agent concentration in gray matter (blue) and white matter (orange) and the approximated linear relation (dotted line). Abbreviations: SI, signal intensity with the presence of the contrast agent; SO, native tissue signal intensity

Contrast agent administration

For higher field strengths, the blood and tissue T_1 relaxation time increases, while the relaxivity, r_1 , decreases only slightly compared to 3T. Therefore, at 7T, a lower (e.g., half) dose of the CA was used, that is, 0.05 mmol Gd/kg body weight. This administration of half dose has previously been shown to be effective in improving the vascular input function (VIF) by reducing T_2^* -related signal decay effects in DCE-MRI.^{20,21} Preparatory scans in volunteers with a whole dose showed that the signal was also influenced by the T_2^* -related signal decay and that the half dose was more suitable for this DCE-MRI protocol.

In addition, another setting influencing the signal enhancement is the injection rate of the CA. A lower injection rate provides a longer duration of the CA bolus at the expense of a lower maximum signal and a broader vascular peak.²² With higher injection rates, T_2^* -related signal decay effects would also occur as the bolus peak concentration is proportional to the injection rate.²² Measurements in volunteers showed that at an injection rate of 0.3 ml/s and the half dose, a maximum signal enhancement ($S/S_0 - 1$) of approximately 2 was found (Figure 3B). Based on our computations above, the T_2^* effect is negligible for the corresponding signal changes.

Subjects

For the validation of the DCE-MRI method at 7T, subjects of two studies were included. Ten healthy subjects without comorbidities, from

a cohort investigating the cardiovascular and cerebral changes after preeclampsia, were examined using the DCE-MRI protocol: all females; median age: 39 years; range: 30–44 years.

Additionally, to obtain a wider range of leakage values, two patients with cerebrovascular disease underwent the DCE-MRI protocol: a male, 49 years, scanned 5 months after clinical ischemic stroke, with a lesion in the right occipital and frontal lobes (precentral gyrus and medial frontal gyrus); and another male, 70 years, scanned 3 months after transient ischemic attack, without any visible lesion.

Both studies were approved by the ethics committee of Maastricht University Medical Center (NL47252.068.14 and NL57690.068.16, respectively) and written informed consent was obtained.

Image processing

For an accurate conversion of the T_1 -map signal intensity to concentration, the effect of B_1^+ variation on the signal was removed using the B_1^+ maps obtained by the Sa2RAGE sequence.^{14,23} The T_1 -weighted images were further processed by performing bias field correction, skull stripping, and gradient distortion correction²³ and segmented into the WM, GM, and cortex.²⁴ The stroke lesion was delineated using the T_2 -weighted and FLAIR images.

To correct for head displacements between dynamic acquisitions, all acquired dynamic images were spatially registered to the same reference image, which was chosen as the average image of the precontrast images from the slow part of the DCE-MRI sequence.

The signal drift was assessed in gadolinium phantom vials for all healthy controls and showed a signal decrease of $0.4 \pm 0.02\%$ over time. The blood signal time-course for the VIF was obtained from the SSS.

BBB leakage analysis was performed as previously described.⁶ Voxel-wise pharmacokinetic modeling was applied using the graphical Patlak approach, which provided the BBB leakage rate (slope of the Patlak plot, K_i) and blood plasma volume fraction (intercept, v_p). The outcome measures were calculated per ROI as the mean K_i and v_p .

Statistics

Statistical analyses of the differences in K_i and v_p between WM and GM were assessed. In the control group, K_i and v_p of the GM and WM were tested for normality using a Shapiro–Wilk test. Both K_i and v_p values showed that all regions were normally distributed ($p > 0.06$ and $p > 0.2$, respectively). A paired-samples T-test was performed to investigate differences in K_i and v_p between the GM and WM. Results were considered significant with a threshold of $p < 0.05$.

Given the small number of participants, significant differences in K_i and v_p for each region between the individual patients and the healthy subjects were inferred, in case the values were outside the 95% confidence interval (CI) of the healthy subjects.

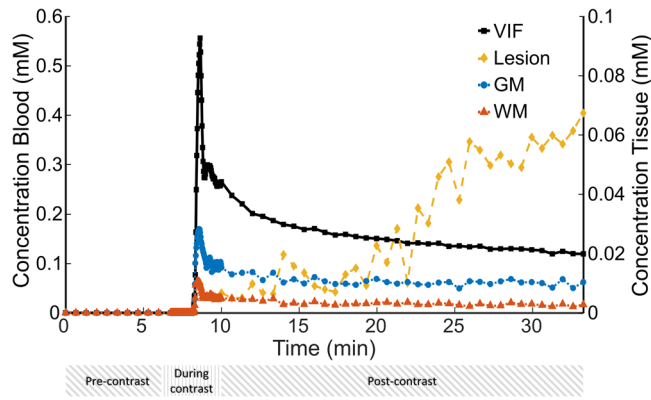


FIGURE 4 Example curves of the contrast agent concentration in blood (black, vascular input function), stroke lesion (yellow), and normal-appearing gray matter (blue) and white matter (red) of an ischemic stroke patient (male, 49 years). Below the time axis, there are bars depicted to indicate the time periods of the fast (during contrast) part and slow (pre and postcontrast) part of the dynamic contrast-enhanced MRI (DCE-MRI) scan. The concentration time-course in the stroke lesion was only measured with the slow (postcontrast) part of the DCE scan as the lesion was outside the field-of-view of the fast DCE scan. Abbreviations: GM, gray matter; VIF, vascular input function; WM, white matter

RESULTS

Examples of the concentration curves obtained in venous blood, the stroke lesion, GM, and WM are shown in Figure 4. CA leakage in GM and WM is small, which is represented by a less steep decline in the postcontrast slow part of the time-course compared to blood, while in the stroke lesion the concentration increases over time.

Examples of Patlak plots in the stroke lesion, GM, and WM and a representative BBB leakage rate map are displayed in Figures 5 and 6, respectively. In the ischemic stroke patient with the visible lesion, a larger BBB leakage in GM compared to WM was observed and the strongest leakage was found in the lesion.

The results of the regional analysis of the DCE-MRI measures are presented in Table 2. For all participants, significantly higher K_i and v_p values were obtained in GM compared to WM ($p = 0.03$

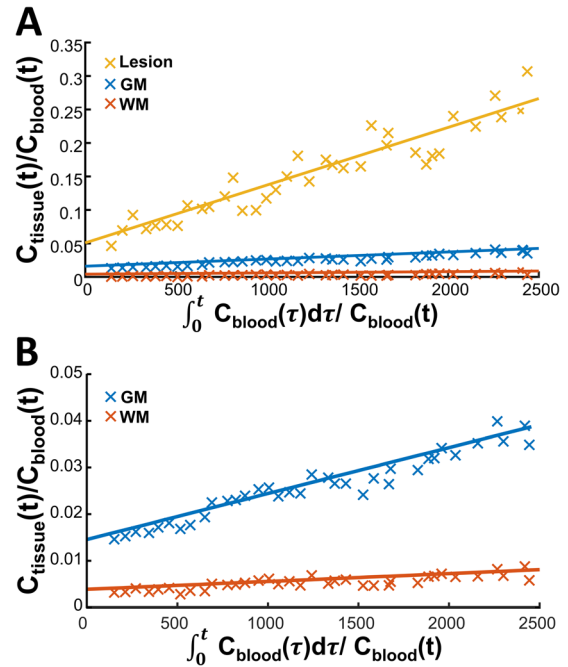


FIGURE 5 Patlak plots of the stroke lesion (yellow), gray matter (blue), and normal-appearing white matter (red) of an ischemic stroke patient (male, 49 years) are depicted in A and we zoomed in on the gray matter (blue) and normal-appearing white matter in B to further visualize the difference between these tissues. Note that the $C_{tissue}(t)/C_{blood}(t)$ range substantially differs between the stroke lesion and the normal-appearing gray matter and white matter tissue. Abbreviations: $C_{blood}(t)$, concentration in the blood; $C_{tissue}(t)$, concentration in the tissue at a certain time point t ; GM, gray matter; WM, white matter

and $p < 0.001$, respectively). In the ischemic stroke patient with an MRI-visible lesion, the leakage rate and blood plasma leakage fraction of the lesion were much higher compared to the nonlesional tissue regions. Furthermore, in both patients with cerebrovascular disease, a higher K_i was found in the nonlesional tissue compared to the control subjects, while no differences in v_p values were detected.

TABLE 2 Regional comparison of DCE-MRI measures: Mean leakage rate values (K_i) and blood plasma volume fraction (v_p) in healthy controls and patients with cerebrovascular disease

	K_i ($\times 10^{-4} \text{ min}^{-1}$)			v_p ($\times 10^{-2}$)		
	Controls	Patient 1	Patient 2	Controls	Patient 1	Patient 2
WM	0.6 ± 0.4 (0.01–1.0)	1.2*	4.2*	0.5 ± 0.1 (0.4–0.6)	0.4	0.6
GM	0.9 ± 1.0 (0.2–2.1)	3.3*	7.4*	1.5 ± 0.2 (1.4–1.6)	1.5	1.4
Cortex	1.2 ± 1.1 (0.2–2.3)	3.6*	7.8*	1.5 ± 0.2 (1.3–1.5)	1.3	1.5
Lesion	N/A	737	NV	N/A	5.1	NV

All data in healthy controls are represented as mean \pm standard deviation with the 95% confidence interval (CI) of the mean in parentheses. Patient 1 was diagnosed with a clinical ischemic stroke with a visible lesion and patient 2 was diagnosed with a transient ischemic attack without a visible lesion.

*Patient-specific values located outside the 95% CI of those of controls.

Abbreviations: GM, gray matter; N/A, not applicable; NV, not visible on MRI; WM, white matter.

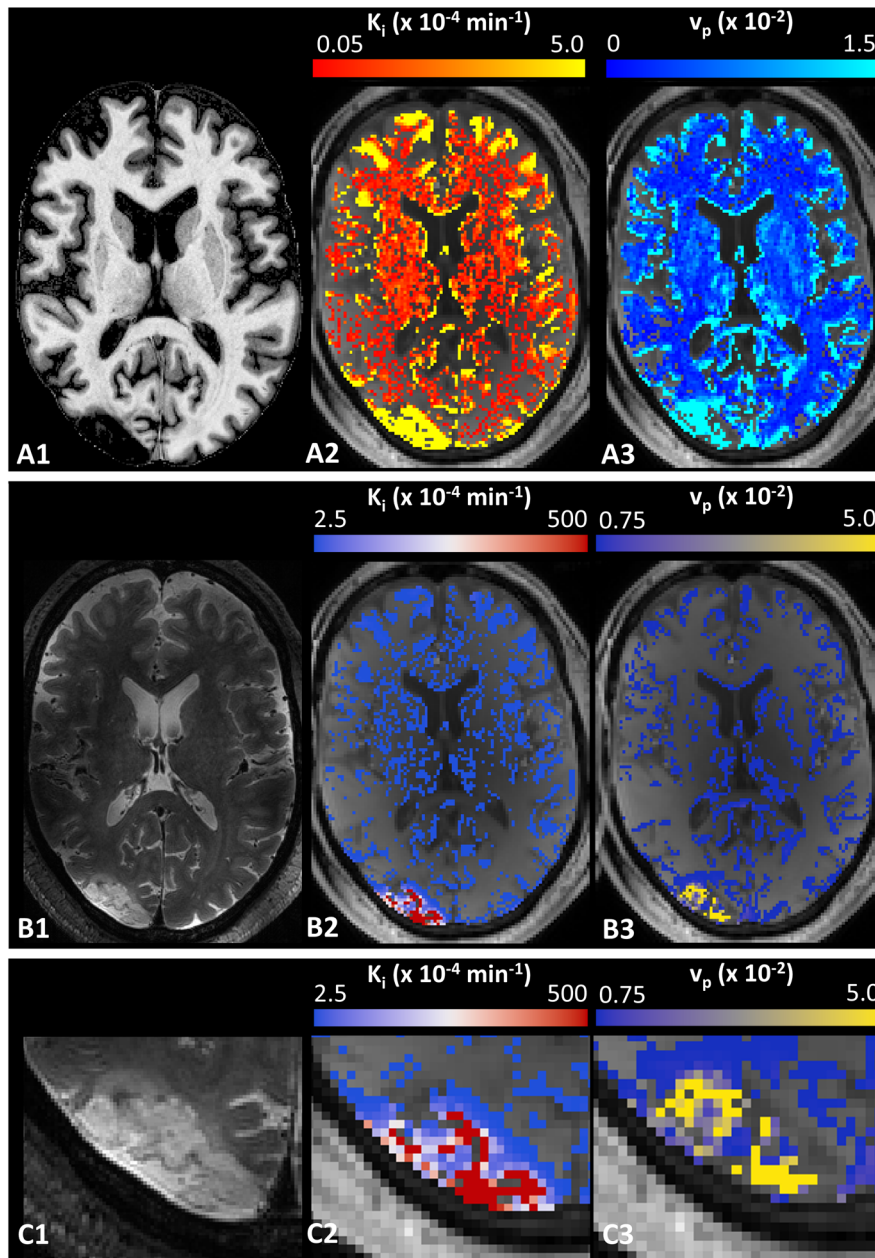


FIGURE 6 T_1 -weighted image, the corresponding slice of a DCE image with a color-coded overlay of the K_i -map and v_p -map of the ischemic stroke patient (male, 49 years, A1–A3). The T_2 -weighted slice with the stroke lesion and the corresponding slice of a DCE image with a color-coded overlay of the K_i -map and v_p -map with a different color-coding range to improve visibility of the leakage in the stroke lesion (B1–B3) and a magnified area of the stroke lesion with the same color-coding range (C1–C3).

DISCUSSION

In this study, we set out to introduce a continuous sampling, dual-time resolution DCE-MRI protocol at 7T to determine subtle leakage of the BBB in healthy subjects and two patients with cerebrovascular disease. T_2^* signal degrading effect of the temporarily high concentration in the blood vessels was minimized by using a small dose and slow injection rate of the CA. The applicability of the method was also investigated in two patients with cerebrovascular disease to assess a large range of

leakage measures. Higher leakage rates were found in GM compared to WM in all participants. For the ischemic stroke patient, a higher leakage rate was obtained in the stroke lesion compared to other cerebral tissues. Moreover, the normal-appearing tissue, distant to the stroke lesion, also had higher leakage values in the patients with cerebrovascular disease compared to healthy subjects.

We showed that the measurements were sensitive enough to observe significant differences in K_i values between WM and GM in all participants in agreement with biological expectations. In histological



and in vivo imaging studies, it has been shown that the vascular volume in GM is higher compared to WM.^{25,26} This is in concordance with our results, which provided higher v_p values in GM than WM. The higher blood vessel surface area of GM results in higher K_i values and explains the higher leakage rates compared to WM.^{25,26}

Although we should be cautious with comparing the K_i values in WM, GM, and the cortex of the two patients with cerebrovascular disease with those of the control subjects, they were higher in the patients and outside the 95% CI of the controls. This higher BBB leakage rate could be explained by either the differences in age²⁷ and/or impaired condition of the microvasculature, which should be investigated in more detail in future studies. Furthermore, we observed much higher K_i values in the stroke lesion compared to the normal-appearing tissue. These results are in line with other studies, which also performed DCE-MRI and pharmacokinetic modeling at 1.5T and 3T.^{11,28} The K_i and v_p values obtained in the stroke lesion were larger compared to other studies at 3T.^{11,28} Comparison of leakage measures in normal-appearing tissues, in healthy controls and in patients with cerebrovascular disorders, obtained in this study with other studies performed at 3T, provided values in the same order using a comparable scan methods.^{6,11,19,28} As DCE-MRI at 7T is expected to be more sensitive for subtle BBB leakage, the difference in leakage values between a stroke lesion and normal-appearing tissues is also expected to be more accurate. However, results should not (yet) be considered as fully quantitative measures, as they vary between research labs, studies, scan protocols, and analysis methods.^{29,30}

Moving from 3T to 7T could possibly detect more subtle BBB leakage. While results could not be compared directly, computer simulations already showed that due to differences in field strength characteristics, such as relaxation times and CA relaxivity, the maximal signal enhancement increases from 2.6 at 3T to 3.5 at 7T. Moreover, another benefit of 7T MRI is that it allows the acquisition of images with higher spatial and temporal resolution. The current continuously sampling dual-time resolution DCE-MRI protocol at 7T had higher spatial and temporal resolutions of the scans during the CA administration and slightly lower spatial and temporal resolutions for the pre/postcontrast scans compared with 3T^{5,27,31} (e.g., voxel size: $1.5 \times 1.5 \times 1.5 \text{ mm}^3$; dynamic scan interval: 34 s for the pre and postcontrast scans, and voxel size: $2 \times 2 \times 2 \text{ mm}^3$; dynamic scan interval: 1.86 s for the scans during contrast administration at 7T vs voxel size: $1 \times 1 \times 2 \text{ mm}^3$; dynamic scan interval: 30.5 s for the pre and postcontrast scans, and voxel size: $2 \times 2 \times 5 \text{ mm}^3$; dynamic scan interval: 3.2 s for the scans during contrast administration). Thus, although results between 3T and 7T were not directly obtained in the same subjects, improved possibilities of 7T DCE-MRI can be pointed out.

DCE-MRI for measuring BBB integrity has been increasingly applied in recent years using 1.5T and 3T MRI systems for research on cerebrovascular, neurodegenerative, and other disorders.^{6,11,32,33} However, to date, only three studies using DCE-MRI at 7T for assessing BBB integrity have been published. In the first study, the contrast enhancement of active MS lesions revealed BBB opening with a T_1 -weighted DCE-MRI sequence acquired at multiple, variable time-points up to 30 min after CA administration.³⁴ In another study, using FLAIR images

of patients with spontaneous intracerebral hemorrhage, the extent of CA leakage distant from the hematoma was shown.³⁵ However, both studies did not correct for the vascular supply of the CA. A quantitative pharmacokinetic analysis of DCE-MRI requires a, preferably subject-specific, VIF, which is ideally obtained from a cerebral artery. However, when assessing the CA concentration in arteries, such as the basilar artery, partial volume effects hinder to obtain a suitable arterial input function. Therefore, we obtained the VIF from the SSS, which was previously found favorable due to a higher consistency.³⁶ The latter study using 7T DCE-MRI showed comparable K_i and v_p values of WM and GM with our current study.³⁷ Note that the study by van den Kerkhof et al. performed a sparsely time-sampled DCE-MRI protocol in healthy subjects. To our knowledge, the current study is the first study with a continuous sampling, dual-time resolution DCE-MRI protocol at 7T combined with pharmacokinetic modeling to assess subtle BBB leakage.

Although several challenges occur when moving to higher field strengths, the current study has demonstrated that most of them can be overcome with the introduced DCE-MRI protocol and analysis pipeline. One of the main advantages of DCE-MRI at a higher magnetic field strength is that it provides a higher SNR. This is also why a lower CA dose (0.05 mmol Gd/kg body weight) was administered than normally clinically used (0.1 mmol Gd/kg body weight). Moreover, the clinically injected CA dose was not suitable, because with that dose, the signal intensity changes were clearly affected with T_2^* signal decay, and the CA concentration could not be estimated accurately. This reduction in CA dose at 7T reduces the potential CA-associated health risks, such as nephrogenic systemic fibrosis³⁸ and long-term tissue accumulation after repeated gadolinium injections.³⁹

DCE-MRI studies at 3T often use an injection rate of 3.0 ml/s to obtain a sharp CA bolus.^{19,33,40} In the preparatory phase of this study at 7T, we found that an injection rate of 3.0 ml/s in combination with our DCE-sequence resulted in signal enhancement with a substantial T_2^* signal decay. This T_2^* induced signal degradation gives rise to an underestimation of CA concentration, hampering the accurate determination of BBB permeability measures. At a lower injection rate of 0.3 ml/s, this T_2^* signal decay could be neglected and was, therefore, used. However, from a physiological perspective, it is in theory beneficial to create a strong concentration gradient between the blood space and brain parenchyma to stimulate the leakage of the CA. In future studies, the optimal CA injection rate at 7T needs to be investigated in more detail.

Another potential complication of 7T compared to lower field strengths is the intrinsically stronger inhomogeneity of the B_0 and B_1 field. Due to these inhomogeneities, the SNR varies across brain regions and may affect the local detection limit of leaking CA. However, these inhomogeneities do not vary over time and the leakage measure is calculated from temporal changes of the signal in the same voxels. It remains to be shown how strong the biological spatial variation in leakage is in comparison to the spatial variation in detection limit.

While the changes in signal intensity in normal-appearing tissues are up to 20%, we found a negligible signal drift over time in gadolinium phantom vials (e.g., -0.4%). Unfortunately, the signal drift is rarely reported in DCE-MRI. Cramer et al. reported a 1–3% drift at 3T over



15 min,⁴¹ which is slightly higher compared to our signal drift, while Varatharaj et al. reported a drift similar to ours.³³ Therefore, no correction for drift was applied for assessing BBB permeability measures.

The current study has some potential limitations. First, this was a study with a small sample size. Also, control subjects and patients were not well matched regarding age and sex. However, despite the low number of participants, this technique showed to be suitable to study subtle as well as clinically relevant differences in BBB permeability.

Additionally, a long (27-min) acquisition time of the continuous sampling DCE-MRI sequence at 7T is used to assess the integrity of the BBB. This acquisition time might be too long to be applied in a clinical setting. Previously, with data acquired at 3T, more accurate leakage results could be obtained with such long acquisition times,^{19,41} and most current DCE-MRI studies at 3T have acquisition times between 20 and 30 min,^{6,11,18,31} similar to our continuous sampling DCE-MRI sequence at 7T. Also, in another 7T MRI study, it was shown that a sparsely time-sampled DCE-MRI protocol with a time interval of approximately 20 min could detect subtle BBB leakage.³⁷ In the future, the sensitivity for detecting subtle BBB leakage at shorter acquisition times should also be investigated with our continuously sampling DCE-MRI protocol to see whether the acquisition time can be shortened.

The settings for the scanning parameters and contrast administration were based on theoretical calculations. Further empirical optimization of these settings might improve the sensitivity for BBB permeability measurements. However, optimization of the protocol requires multiple CA injections in the same volunteer, which is difficult to implement because of ethical constraints due to potential CA-associated health risks, which also complicates face-to-face comparison of 3T and 7T.

To conclude, we demonstrated that assessment of BBB integrity at 7T with a continuous sampling DCE-MRI sequence is feasible. A low dose and slow injection rate are advised for the CA bolus to avoid T_2^* signal artifacts that may comprise the signal to concentration conversion. The described protocol combined with pharmacokinetic modeling was shown to detect subtle differences in leakage between WM and GM, as well as cerebrovascular compromised tissue. In the future, DCE-MRI at 7T has potential to provide valuable information and better pathological understanding of disorders. In particular, in MS, it could specifically be valuable for stratification of lesion tissue types (WM vs. GM-lesions), or tissues classes (e.g., cortex vs. deep GM vs. thalamus).

ACKNOWLEDGMENT AND DISCLOSURE

The authors thank Joost de Jong, Kim Bekelaar, Inger de Ridder, and Julie Staals for help with data acquisition and data analysis. We also thank the members of the DECONNECT consortium: Suzanne Gerretsen, Petra Hurks, Eline Kooi, and Eva Mulder for their help with the study. Finally, we thank the Brains Unlimited Pioneer Fund (reference S.2016.1.06) and the Stimulation Fund (Stimuleringsfonds FHML) of the Maastricht University for providing financial support to this project.

ORCID

Lisanne P. W. Canjels  <https://orcid.org/0000-0003-4880-2670>

Jacobus F. A. Jansen  <https://orcid.org/0000-0002-5271-8060>

Marieke van den Kerkhof  <https://orcid.org/0000-0002-6849-4751>

REFERENCES

- Heye AK, Culling RD, Valdés Hernández MDC, Thrippleton MJ, Wardlaw JM. Assessment of blood–brain barrier disruption using dynamic contrast-enhanced MRI. A systematic review. *Neuroimage Clin* 2014;6:262-74.
- Jain R. Measurements of tumor vascular leakiness using DCE in brain tumors: clinical applications. *NMR Biomed* 2013;26:1042-9.
- Jelescu IO, Leppert IR, Narayanan S, Araújo D, Arnold DL, Pike GB. Dual-temporal resolution dynamic contrast-enhanced MRI protocol for blood–brain barrier permeability measurement in enhancing multiple sclerosis lesions. *J Magn Reson Imaging* 2011;33:1291-300.
- Merali Z, Huang K, Mikulis D, Silver F, Kassner A. Evolution of blood–brain-barrier permeability after acute ischemic stroke. *PLoS One* 2017;12:e0171558.
- Wong SM, Jansen JFA, Zhang CE, et al. Blood–brain barrier impairment and hypoperfusion are linked in cerebral small vessel disease. *Neurology* 2019;92:e1669-77.
- van de Haar HJ, Burgmans S, Jansen JFA, et al. Blood–brain barrier leakage in patients with early Alzheimer disease. *Radiology* 2016;281:527-35.
- Vaughan JT, Garwood M, Collins CM, et al. 7T vs. 4T: RF power, homogeneity, and signal-to-noise comparison in head images. *Magn Reson Med* 2001;46:24-30.
- Schmitter S, Moeller S, Wu X, Auerbach EJ, Metzger GJ. Simultaneous multislice imaging in dynamic cardiac MRI at 7T using parallel transmission. *Magn Reson Med* 2017;77:1010-20.
- Hagberg GE, Scheffler K. Effect of r_1 and r_2 relaxivity of gadolinium-based contrast agents on the T_1 -weighted MR signal at increasing magnetic field strengths. *Contrast Media Mol Imaging* 2013;8:456-65.
- Hylton N. Dynamic contrast-enhanced magnetic resonance imaging as an imaging biomarker. *J Clin Oncol* 2006;24:3293-8.
- Heye AK, Thrippleton MJ, Armitage PA, et al. Tracer kinetic modelling for DCE-MRI quantification of subtle blood–brain barrier permeability. *Neuroimage* 2016;125:446-55.
- Tofts PS, Brix G, Buckley DL, et al. Estimating kinetic parameters from dynamic contrast-enhanced T_1 -weighted MRI of a diffusible tracer: standardized quantities and symbols. *J Magn Reson Imag* 1999;10:223-32.
- Teeuwisse WM, Brink WM, Webb AG. Quantitative assessment of the effects of high-permittivity pads in 7 Tesla MRI of the brain. *Magn Reson Med* 2012;67:1285-93.
- Marques JP, Kober T, Krueger G, van der Zwaag W, Van de Moortele PF, Gruetter R. MP2RAGE, a self bias-field corrected sequence for improved segmentation and T_1 -mapping at high field. *Neuroimage* 2010;49:1271-81.
- Shen Y, Goerner FL, Snyder C, et al. T_1 relaxivities of gadolinium-based magnetic resonance. *Invest Radiol* 2015;50:330-8.
- Rooney WD, Johnson G, Li X, et al. Magnetic field and tissue dependencies of human brain longitudinal H₂O relaxation in vivo. *Magn Reson Med* 2007;57:308-18.
- Ikonomidou VN, van Gelderen P, de Zwart JA, Duyn JH. T_1 measurements at 7T with application to tissue specific imaging. *Proc Int Soc Magn Reson Med* 2006;251:920.
- Starr JM, Farrall AJ, Armitage P, McGurn B, Wardlaw J. Blood–brain barrier permeability in Alzheimer's disease: a case–control MRI study. *Psychiatry Res - Neuroimaging* 2009;171:232-41.



19. van de Haar HJ, Jansen JFA, Jeukens CRLPN, et al. Subtle blood–brain barrier leakage rate and spatial extent: considerations for dynamic contrast-enhanced MRI: considerations. *Med Phys* 2017;44:4112-25.
20. Filice S, Crisi G, Erb G. T_2^* -Correction in dynamic contrast-enhanced magnetic resonance imaging of glioblastoma from a half dose of high-relaxivity contrast agent. *J Comput Assist Tomogr* 2017;41:916-21.
21. Nijenhuis RJ, Gerretsen S, Leiner T, Jacobs MJ, Engelshoven JMA Van, Backes WH. Gadobutrol for magnetic resonance angiography of the supplying arteries of the spinal cord in thoracoabdominal aortic aneurysm patients. *J Magn Reson Imaging* 2005;22:136-44.
22. Carroll TJ, Korosec FR, Swan JS, Hany TF, Grist TM, Mistretta CA. The effect of injection rate on time-resolved contrast-enhanced peripheral MRA. *J Magn Reson Imaging* 2001;14:401-10.
23. Haast RAM, Ivanov D, Formisano E, Uludağ K. Reproducibility and reliability of quantitative and weighted T_1 and T_2^* mapping for myelin-based cortical parcellation at 7 Tesla. *Front Neuroanat* 2016;10:112.
24. Fischl B, Salat DH, Busa E, et al. Whole brain segmentation: automated labeling of neuroanatomical structures in the human brain. *Neuron* 2002;33:341-55.
25. Leenders KL, Perani D, Lammertsma AA, et al. Cerebral blood flow, blood volume and oxygen utilization. Normal values and effect of age. *Brain* 1990;113:27-47.
26. Lierse W, Horstmann E. Quantitative anatomy of the cerebral vascular bed with especial emphasis on homogeneity and inhomogeneity in small parts of the gray and white matter. *Acta Neurol Scand Suppl* 1965;14:15-9.
27. Verheggen ICM, de Jong JJA, van Boxtel MPJ, et al. Imaging the role of blood–brain barrier disruption in normal cognitive ageing. *Geroscience* 2020;42:1751-64.
28. Villringer K, Sanz Cuesta BE, Ostwaldt A-C, et al. DCE-MRI blood–brain barrier assessment in acute ischemic stroke. *Neurology* 2017;88:433-40.
29. Raja R, Rosenberg GA, Caprihan A. MRI measurements of blood–brain barrier function in dementia: a review of recent studies. *Neuropharmacology* 2018;134:259-71.
30. Thrippleton MJ, Backes WH, Sourbron S, et al. Quantifying blood–brain barrier leakage in small vessel disease: review and consensus recommendations. *Alzheimers Dement* 2019;15:840-58.
31. Zhang CE, Wong SM, Uiterwijk R, et al. Blood–brain barrier leakage in relation to white matter hyperintensity volume and cognition in small vessel disease and normal aging. *Brain Imaging Behav* 2019;13:389-95.
32. Cramer SP, Simonsen H, Frederiksen JL, Rostrup E, Larsson HBW. Abnormal blood–brain barrier permeability in normal appearing white matter in multiple sclerosis investigated by MRI. *Neuroimage Clin* 2014;4:182-9.
33. Varatharaj A, Liljeroth M, Darekar A, Larsson HBW, Galea I, Cramer SP. Blood–brain barrier permeability measured using dynamic contrast-enhanced magnetic resonance imaging: a validation study. *J Physiol* 2019;597:699-709.
34. Gaitán MI, Sati P, Inati SJ, Reich DS. Initial investigation of the blood–brain barrier in MS lesions at 7 Tesla. *Mult Scler* 2013;19:1068-73.
35. Jolink WMT, Lindenholtz A, van Etten ES, et al. Contrast leakage distant from the hematoma in patients with spontaneous ICH: a 7 T MRI study. *J Cereb Blood Flow Metab* 2020;40:1002-11.
36. Keil VC, Mädler B, Gieseke J, et al. Effects of arterial input function selection on kinetic parameters in brain dynamic contrast-enhanced MRI. *Magn Reson Imaging* 2017;40:83-90.
37. van den Kerkhof M, Voortier PHM, Canjels LPW, et al. Time-efficient measurement of subtle blood–brain barrier leakage using a T_1 mapping MRI protocol at 7T. *Magn Reson Med* 2021;85:2761-70.
38. Grobner T. Gadolinium – a specific trigger for the development of nephrogenic fibrosing dermopathy and nephrogenic systemic fibrosis? *Nephrol Dial Transplant* 2006;21:1104-8.
39. Ramalho J, Semelka RC, Ramalho M, Nunes RH, AlObaidy M, Castillo M. Gadolinium-based contrast agent accumulation and toxicity: an update. *Am J Neuroradiol* 2016;37:1192-8.
40. Larsson C, Kleppetø M, Rasmussen I, et al. Sampling requirements in DCE-MRI based analysis of high grade gliomas: simulations and clinical results. *J Magn Reson Imaging* 2013;37:818-29.
41. Cramer SP, Larsson HB. Accurate determination of blood–brain barrier permeability using dynamic contrast-enhanced T_1 -weighted MRI: a simulation and in vivo study on healthy subjects and multiple sclerosis patients. *J Cereb Blood Flow Metab* 2014;34:1655-65.

How to cite this article: Canjels, LPW, Jansen, JFA, van den Kerkhof, M, Alers, R-J, Poser, BA, Wiggins, CJ, et al. 7T dynamic contrast-enhanced MRI for the detection of subtle blood–brain barrier leakage. *J Neuroimaging*. 2021;31:902–911. <https://doi.org/10.1111/jon.12894>